Check for updates

JGR Atmospheres

RESEARCH ARTICLE
10.1029/2026JD047900

How Does Terrain Relief of the Tibetan Plateau and the Yunnan–Guizhou Plateau Individually Modulate Summer Regional Hourly Extreme Precipitation in the Sichuan Basin, China?

Xiaoke Xu[1], Anning Huang[2,3], Chunlei Gu[2], and Yan Zhang[4]

[1]School of Computer, Chengdu University of Information Technology, Chengdu, China, [2]School of Atmospheric Sciences, Nanjing University, Nanjing, China, [3]Plateau Atmosphere and Environment Key Laboratory of Sichuan Province, College of Atmospheric Sciences, Chengdu University of Information Technology, Chengdu, China, [4]Key Laboratory of Radiometric Calibration and Validation for Environmental Satellites, National Satellite Meteorological Center, China Meteorological Administration (LRCVES/CMA), FengYun Meteorological Satellite Innovation Center (FY-MSIC), Beijing, China

Abstract The influence of terrain relief over the Tibetan Plateau (TP) and the Yunnan–Guizhou Plateau on summer regional hourly extreme precipitation (RHEP) in the Sichuan Basin (SCB) under two dominant synoptic patterns remains poorly understood. Here, this study uses multi-case Weather Research and Forecasting sensitivity experiments, in which the terrain relief of two plateaus is individually smoothed, to systematically investigate these modulation mechanisms. Terrain relief modulates low-level flow and moisture, altering thermodynamic and dynamic processes of RHEP under different synoptic patterns. Under P1, featured by a westerly trough and a southwest vortex over western SCB, the terrain relief over the TP (Yunnan–Guizhou Plateau) prolongs the mean RHEP duration by 3.4 hr (0.6 hr) and increases the mean intensity by 0.38 mm hr^{-1} (0.24 mm hr^{-1}) over the western SCB. The prolonged duration and heightened intensity of RHEP are driven by the intensification of the westerly trough and southwest vortex, a process triggered by enhanced atmospheric baroclinicity, low-level convergence, and vertical-motion forcing induced by terrain relief. Under P2, characterized by a westerly trough and a southwest vortex over central-eastern SCB, the terrain relief over the TP prolongs the RHEP duration by 1.3 hr and increases the intensity by 0.07 mm hr^{-1} over eastern SCB through mechanisms similar to those under P1, but the weakened westerly winds over southeastern SCB limit the enhancement. In contrast, the terrain relief over the Yunnan–Guizhou Plateau reduces the RHEP intensity by 0.32 mm hr^{-1} via strengthening anomalous northerly winds, blocking southwesterly moisture transport, weakening the westerly trough, and suppressing the southwest vortex.

Plain Language Summary Regional hourly extreme precipitation (RHEP) events often cause floods and other disasters in the Sichuan Basin (SCB). The basin is surrounded by the Tibetan Plateau (TP) to the west and the Yunnan–Guizhou Plateau to the south, but how the terrain relief over these plateaus affects RHEP in the basin is still not fully understood. In this study, we used a weather model to compare the real terrain and simulations in which the terrain relief over each plateau is smoothed. This allowed us to examine the separate effects of the terrain relief over the two plateaus under two common weather patterns. We found that terrain relief over the TP generally increases the duration and intensity of RHEP in the western SCB by strengthening upward motion and the southwest vortex, an important rain-producing weather system in southwest China. Terrain relief over the Yunnan–Guizhou Plateau has different effects under different weather patterns. It can enhance RHEP when moisture transport favors the western SCB, but it can weaken RHEP when it blocks southwesterly moisture flow into the eastern SCB. These results show that terrain relief around the SCB can either enhance or suppress extreme rainfall depending on the background weather pattern.

Key Points:

- Tibetan Plateau (TP)/Yunnan–Guizhou Plateau (YGP) terrain relief alters Sichuan Basin (SCB) regional hourly extreme precipitation (RHEP)
- Under a western SCB trough-vortex, TP, and YGP terrain relief increase RHEP via stronger baroclinicity and dynamic forcing
- Under a central-eastern SCB trough-vortex, TP terrain relief weakly increases RHEP; YGP terrain relief curbs it by blocking moisture

Supporting Information:

Supporting Information may be found in the online version of this article.

Correspondence to:

A. Huang,
anhuang@nju.edu.cn

Citation:

Xu, X., Huang, A., Gu, C., & Zhang, Y. (2026). How does terrain relief of the Tibetan Plateau and the Yunnan–Guizhou Plateau individually modulate summer regional hourly extreme precipitation in the Sichuan Basin, China? *Journal of Geophysical Research: Atmospheres*, *131*, e2026JD047900. https://doi.org/10.1029/2026JD047900

Received 23 JUN 2026
Accepted 18 OCT 2026

Author Contributions:

Conceptualization: Anning Huang
Data curation: Xiaoke Xu, Chunlei Gu
Formal analysis: Xiaoke Xu, Anning Huang, Yan Zhang
Investigation: Xiaoke Xu, Anning Huang, Chunlei Gu, Yan Zhang
Methodology: Xiaoke Xu
Resources: Xiaoke Xu, Anning Huang, Chunlei Gu
Software: Xiaoke Xu
Supervision: Anning Huang
Validation: Xiaoke Xu, Anning Huang
Visualization: Xiaoke Xu
Writing – original draft: Xiaoke Xu, Anning Huang
Writing – review & editing: Xiaoke Xu, Anning Huang, Chunlei Gu, Yan Zhang

© 2026 American Geophysical Union. All rights reserved, including rights for text and data mining and training of artificial intelligence technologies or similar technologies.

1. Introduction

Regional hourly extreme precipitation (RHEP), with its extensive spatial influence and prolonged duration, frequently triggers mountain floods, soil erosion, and urban waterlogging. It has become a major focus of recent research (Ali et al., 2021; Bai et al., 2025; Barbero et al., 2019; Q. Li et al., 2022; Yuan et al., 2021). The Tibetan Plateau (TP) and the Yunnan–Guizhou Plateau, featured by multi-scale terrains, encircle the Sichuan Basin

21698996, 2026, 21, Downloaded from https://agupubs.onlinelibrary.wiley.com/doi/10.1029/2026JD047900 by Anning Huang - Nanjing University , Wiley Online Library on [29/10/2026]. See the Terms and Conditions (https://onlinelibrary.wiley.com/terms-and-conditions) on Wiley Online Library for rules of use; OA articles are governed by the applicable Creative Commons License

(SCB). This complex topography favors frequent RHEP in the SCB, yet the underlying physical mechanisms remain unclear (Qian et al., 2015; X. Y. Zhou & Lei, 2018). In particular, the dynamic and thermal effects of the terrain relief on RHEP are critical for improving the physical understanding of extreme precipitation (Houze, 2012; Schröer & Kirchengast, 2018).

Previous studies identify two typical synoptic patterns dominating the occurrence of the RHEP in the SCB (Ng et al., 2021; Nie & Sun, 2021; X. Xu et al., 2023). In the first pattern (hereinafter referred to as P1), the South Asian High expands northeastward, and the West North Pacific Subtropical High (WNPSH) extends northwestward relative to their climatic states (Hu et al., 2015; J. Li et al., 2024; R. Xia et al., 2021). A westerly trough lies over the western SCB, accompanied by a southwest vortex over the western SCB and enhanced moisture transport by southerly winds (F. Xia et al., 2025; Y. Zhang et al., 2021). In the second pattern (hereinafter referred to as P2), the South Asian High expands southeastward and the WNPSH shifts southwestward relative to their climatic states (Cheng et al., 2023; K. Q. Yang et al., 2023). The westerly trough is located over the central-eastern SCB, with a southwest vortex over the central-eastern SCB and the moisture transport driven by southwesterly winds (Deng et al., 2022; S. Zhang et al., 2021). However, most studies primarily focus on these synoptic systems and do not adequately elucidate the mechanisms by which complex terrain influences RHEP.

Some studies also examine the mechanisms by which large-scale terrain influences RHEP (F. Xia et al., 2025; X. Xu et al., 2024). Thermally, the TP and the Yunnan–Guizhou Plateau establish a plateau-basin thermal contrast with the SCB, which enhances stratification instability over the basin and favors the development of the southwest vortex (Liao et al., 2025; Yan et al., 2025). Dynamically, these plateaus jointly form a windward slope along the western SCB, forcing moisture airflow to ascend and thereby inducing RHEP (B. Chen et al., 2024; Zhao, 2015). However, existing studies largely emphasize the effects of large-scale terrain alone and mainly address whether such terrain favors RHEP occurrence (X. Xu et al., 2024, 2025). For further improvement in the physical understanding and predictive skill of RHEP, consideration of terrain relief influence on RHEP is necessary (L. Li & Zhang, 2023).

Previous studies also provide partial insight into the mechanisms by which the terrain relief influences extreme precipitation over the SCB (Gu et al., 2021; J. Li et al., 2025; Z. Wu et al., 2022). Most studies suggest that these effects primarily involve gravity-wave disturbances, convective triggering, and the modulation of near-surface moisture transport (Ji et al., 2026; Y. J. Wang et al., 2025; Yepes et al., 2020). Gravity waves are generated as airflow passes over terrain relief (Liu et al., 2018; Vosper et al., 2018). Under the influence of undulating terrain, gravity waves propagate upward and break, releasing energy, modifying local circulation, and creating favorable dynamical conditions for convective development (Z. Chen et al., 2025; Y. Xu et al., 2025). In addition, terrain relief forces airflow to ascend, and once a critical height is reached, latent heat release enhances instability and triggers convective systems (Mo et al., 2024; C. Shen et al., 2022). Surface friction associated with such terrains slows moisture transport and alters the intensity and duration of extreme precipitation (J. Shen et al., 2025; Y. Wang et al., 2020; A. Wu & Li, 2022; X. Y. Zhou & Li, 2024). However, existing studies mainly focus on individual terrain features or single synoptic backgrounds, and lack systematic comparisons of the different effects of terrain relief on extreme precipitation under different synoptic patterns (Roe, 2005; Yu et al., 2020).

Motivated by the limitations of previous studies mentioned above, this study systematically investigates the mechanisms by which the terrain relief over the TP and the Yunnan–Guizhou Plateau influence RHEP in the SCB under the two dominant synoptic patterns. Based on these synoptic patterns and RHEP events identified by X. Xu et al. (2023, 2025), the Weather Research and Forecasting (WRF) model is employed to conduct sensitivity experiments in which the terrain relief over the TP and the Yunnan–Guizhou Plateau is smoothed. This study addresses the key scientific question as follows: (a) How does terrain relief over the TP and the Yunnan–Guizhou Plateau individually modulate summer RHEP events in the SCB? (b) What are the thermodynamic and dynamic responses of RHEP to terrain relief under distinct dominant synoptic patterns? By elucidating these physical processes, this study clarifies the interactions among topography, atmospheric circulation, and precipitation, and enhances the physical understanding of summer extreme precipitation over the SCB.

2. Background, Data, Numerical Experiments, and Methods

2.1. Background

Following X. Xu et al. (2023), hourly extreme precipitation is first identified at each grid point using the local 95th percentile threshold of summer hourly precipitation during 2000–2020. The number of grid points experiencing hourly extreme precipitation is then counted at each hour, and an RHEP event is identified when this number exceeds its historical 95th percentile threshold over the SCB. This study is based on the two synoptic patterns (P1 and P2) identified by X. Xu et al. (2023) as the dominant large-scale controls of summer RHEP events over the SCB. Detailed descriptions of the synoptic configurations are provided in Figure 1 of X. Xu et al. (2025). For each synoptic pattern, 10 typical and temporally continuous RHEP events are selected for analysis with durations ranging from 14 to 55 hr under P1 and generally from 15 to 21 hr under P2 (Table 1 of X. Xu et al. (2025)). Although the individual cases differ in duration and precipitation intensity, the selected cases under each synoptic pattern share similar precipitation-center locations and large-scale circulation configurations.

2.2. Data

The data used in this study are as follows

1. The 6-hourly FNL global reanalysis, with a horizontal resolution of 1° × 1° and 26 vertical pressure levels, provides the initial and boundary conditions for the numerical simulations (Huang & Gao, 2018).
2. The hourly ERA5 reanalysis data, available at 0.25° horizontal resolution (Hersbach et al., 2020) during the 20 RHEP events selected in this study, are used to evaluate the model performance in reproducing large-scale atmospheric circulation features.
3. The precipitation data of the final-run GPM-IMERG V06 product with 30-min temporal resolution and 0.1° × 0.1° spatial resolution are employed to assess the ability of the model to simulate precipitation (Hou et al., 2014). Previous studies demonstrate that this data set reliably captures the spatial distribution, temporal evolution, and magnitude of extreme rainfall in the SCB (Fang et al., 2019; C. Shen et al., 2022; M. Yang et al., 2020). Using observations from stations over the SCB during 2000–2020, we verified that GPM reasonably reproduces the spatial distribution of station-based 95th-percentile extreme precipitation (Figure S1 in Supporting Information S1).

2.3. Numerical Experiments

This study employs version 4.2 of the WRF model developed by the National Center for Atmospheric Research (Skamarock et al., 2019). The control experiment (CTL) is conducted with real terrain (Figure 1a). This study used FNL data for the initial and lateral boundary conditions. FNL outperformed ERA5 in reproducing GPM accumulated precipitation, with spatial correlation coefficients of 0.47 and 0.35, respectively, over 102°E–108°E, 29°N–33°N (Figure S2 in Supporting Information S1). The WRF model configuration and physical parameterization schemes are summarized in Table 1.

Following X. Xu et al. (2025), different physical parameterization combinations are adopted for P1 and P2 because previous sensitivity tests showed that the optimal schemes differ between the two synoptic patterns. For all simulations under the same synoptic pattern, the CTL and sensitivity experiments use identical model configurations and physical parameterization schemes; therefore, their differences mainly reflect the effects of terrain relief.

All sensitivity experiments use the same model configuration as the CTL experiment and differ only in model-resolved terrain treatment. Terrain elevation within a target region is smoothed through repeated nine-point smoothing to suppress terrain relief variability while retaining the large-scale terrain structure. After each iteration, the terrain standard deviation, defined as the spatial standard deviation of 3 × 3 grid point elevations within the modified region, is recalculated (Y. Wu et al., 2018; X. Xu et al., 2023). The smoothing was repeated until the regional mean of the 3 × 3 local terrain standard deviation within the target region is lower than 100 m (Pielke, 2013). In the TP_NM experiment, the smoothing is applied to the TP region (85°E–104.5°E, 27°N–40°N) (Figure 1b). In the YG_NM experiment, the same procedure is applied to the Yunnan–Guizhou Plateau region (90°E–107°E, 20°N–28°N) (Figure 1c).

21698996, 2026, 21, Downloaded from https://agupubs.onlinelibrary.wiley.com/doi/10.1029/2026JD047900 by Anming Huang - Nanjing University , Wiley Online Library on [29/10/2026]. See the Terms and Conditions (https://onlinelibrary.wiley.com/terms-and-conditions) on Wiley Online Library for rules of use; OA articles are governed by the applicable Creative Commons License

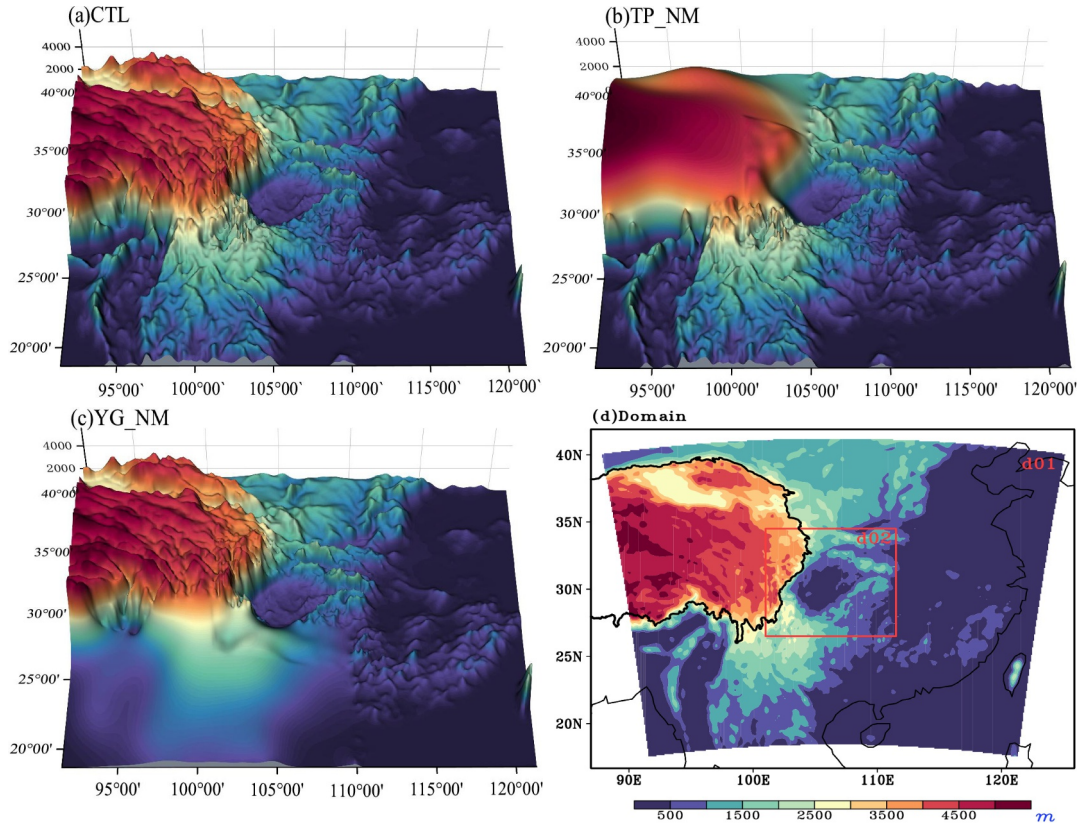


Figure 1. Three-dimensional distribution of terrain (shading, unit: m) and the nesting strategy of the numerical model. The real terrain in the CTL experiment (a). The TP_NM experiment smooths the terrain relief over the Tibetan Plateau within the region of 85°E–104.5°E, 27°N–40°N (b). The YG_NM experiment smooths the terrain relief over the Yunnan–Guizhou Plateau within the region of 90°E–107°E, 20°N–28°N (c). The terrain distribution in the numerical model and nesting strategy (d).

Table 1
Weather Research and Forecasting (WRF) Model Configuration and Physical Parameterization Schemes

Category	Configuration	
Model	WRF-ARW version 4.2	
Nesting strategy	Two-way nesting with two domains	
Horizontal resolution	18 and 6 km for the outer and inner domains	
Grid points	181 × 144 and 208 × 175 for the outer and inner domains	
Domain center	29.83°N, 106.46°E	
Vertical levels	41	
Time step	30 s	
Spin-up time	12 hr	
Physical parameterization	P1	P2
Planetary boundary layer	Yonsei University scheme	ACM2 scheme
Microphysics	Morrison two-moment scheme	WSM3/WSM5 schemes
Radiation	CAM shortwave and longwave schemes	CAM shortwave and longwave schemes
Land surface	Unified Noah land surface model	Unified Noah land surface model
Cumulus parameterization	Grell-Freitas ensemble scheme	Grell-Freitas ensemble scheme

21698996, 2026, 21, Downloaded from https://agupubs.onlinelibrary.wiley.com/doi/10.1029/2026JD047900 by Anning Huang - Nanjing University , Wiley Online Library on [29/10/2026]. See the Terms and Conditions (https://onlinelibrary.wiley.com/terms-and-conditions) on Wiley Online Library for rules of use; OA articles are governed by the applicable Creative Commons License

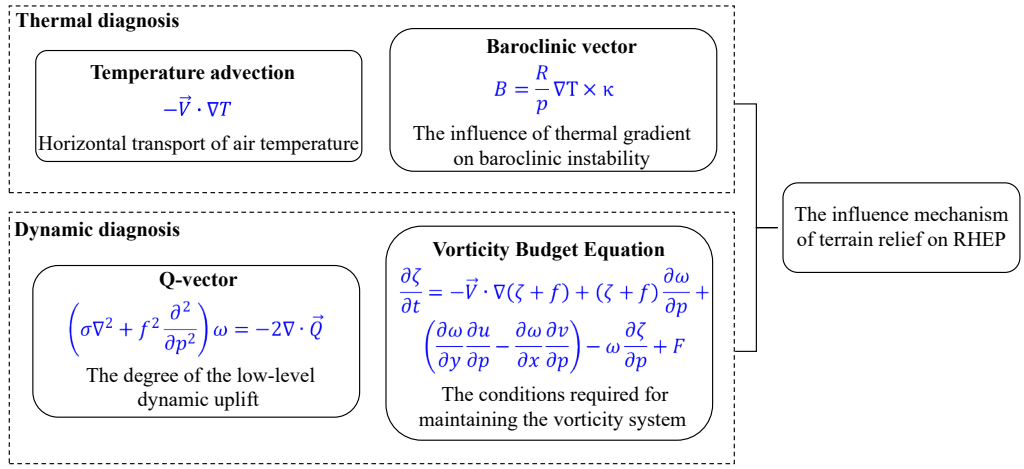


Figure 2. An analysis strategy diagram. Each box indicates the mathematical equations used in this study and their physical meanings. Each symbol represents the meaning and its unit as detailed in Section 2.4.

2.4. Methods

A series of physical equations and quantities is calculated from the perspective of thermal and dynamic diagnosis (Figure 2).

2.4.1. Vorticity Budget Equation

The southwest vortex is the primary weather system affecting RHEP over the SCB. Vorticity budget analysis is a key dynamic tool for understanding the development, maintenance, and extinction of the southwest vortex (Holton & Hakim, 2013). The complete vorticity budget equation is

$$\underset{}{\frac{\partial\zeta}{\partial t}}=\underset{①}{-\vec{V}\cdot\nabla(\zeta+f)}\ \underset{①}{+(\zeta+f)\frac{\partial\omega}{\partial p}}\ \underset{③}{+\left(\frac{\partial\omega}{\partial y}\frac{\partial u}{\partial p}-\frac{\partial\omega}{\partial x}\frac{\partial v}{\partial p}\right)}\ \underset{④}{-\omega\frac{\partial\zeta}{\partial p}}\ \underset{⑤}{+F} \tag{1}$$

Where $\frac{\partial\zeta}{\partial t}$ represents the change rate of vorticity ζ over time t. The first term ① on the right side $-\vec{V}\cdot\nabla(\zeta+f)=-\vec{V}\cdot\nabla\zeta-\beta v$ is the absolute vorticity advection term, which is combined into the horizontal advection term and the beta term. It symbolizes the local vorticity variation caused by the absolute vorticity conveyed by the horizontal wind. $\vec{V}$ represents the wind vector with components u and v in the x and y directions, respectively. $\nabla=\frac{\partial}{\partial x}+\frac{\partial}{\partial y}$ is the gradient operator. $\zeta=\frac{\partial v}{\partial x}-\frac{\partial u}{\partial y}$ is relative vorticity. f is the Coriolis parameter, which varies with latitude. The second term ② $(\zeta+f)\frac{\partial\omega}{\partial p}$ is the divergence term, also called "stretch term." It describes the changes in vertical vorticity compression (stretching) due to the convergence (divergence) of the horizontal wind field. ω denotes the vertical velocity in p coordinate, with p as pressure. The third term ③ $\left(\frac{\partial\omega}{\partial y}\frac{\partial u}{\partial p}-\frac{\partial\omega}{\partial x}\frac{\partial v}{\partial p}\right)$ is a tilting term. It describes the process in which horizontal vorticity is "tilted" into the vertical direction due to uneven vertical motion, thereby changing the vertical vorticity. The $-\omega\frac{\partial\zeta}{\partial p}$ is the vertical advection term ④, which represents the vorticity changes caused by vertical movement transporting vorticity at different heights to the local area. For example, upward motion ($\omega<0$) transports vorticity from the lower layer to the upper layer, increasing the local vorticity. The last term F is the friction residual term. Near-ground friction generates negative vorticity sources, which are referred to as frictional dissipation. The units of each term in the vorticity budget equation are all s^{-2}.

It is essential to note that the analysis in this study is based on the composite mean of multiple RHEP events. Vorticity changes over time are assumed to be zero, and the friction term and residuals are combined, as referenced by Sanders (1986) and Orlanski and Sheldon (1995).

21698996, 2026, 21, Downloaded from https://agupubs.onlinelibrary.wiley.com/doi/10.1029/2026JD047900 by Anning Huang - Nanjing University , Wiley Online Library on [29/10/2026]. See the Terms and Conditions (https://onlinelibrary.wiley.com/terms-and-conditions) on Wiley Online Library for rules of use; OA articles are governed by the applicable Creative Commons License

$$-F + \text{Residual} = -\vec{V} \cdot \nabla(\zeta + f) + (\zeta + f)\frac{\partial \omega}{\partial p} + \left(\frac{\partial \omega}{\partial y}\frac{\partial u}{\partial p} - \frac{\partial \omega}{\partial x}\frac{\partial v}{\partial p}\right) - \omega\frac{\partial \zeta}{\partial p} \quad (2)$$

The analysis results from Equation 2 reflect the vortex system equilibrium state through time averaging, rather than an instantaneous process. Therefore, the physical meaning of the vorticity budget equation used in this study is the advection transport, convergence stretching, tilt effect, and vertical transport required to maintain the quasi-stationary state of the vortex system.

2.4.2. Q-Vector

Extreme precipitation is more directly associated with persistent and strong vertical motion. Diagnosing the forcing mechanisms of terrain on air vertical motion is crucial for understanding the dynamical core of extreme precipitation events. Previous studies usually diagnose vertical motion using the traditional ω equation in p-coordinate (Yao et al., 2012).

$$\left(\sigma\nabla^2 + f^2\frac{\partial^2}{\partial p^2}\right)\omega = \underbrace{f\frac{\partial}{\partial p}\left(\overrightarrow{V_g} \cdot \nabla\zeta\right)}_{①} - \underbrace{\left[\overrightarrow{V_g} \cdot \nabla\left(\frac{\partial \Phi}{\partial p}\right)\right]}_{②} \quad (3)$$

The left side of Equation 3 is the Laplacian term of the vertical velocity. $\sigma\nabla^2$ represents the suppression of vertical motion by static stability. The term $f^2\frac{\partial^2}{\partial p^2}$ reflects the dynamic constraint induced by the vertical shear of geostrophic vorticity. σ denotes the static stability parameter. The first term ① on the right side $f\frac{\partial}{\partial p}\left(\overrightarrow{V_g} \cdot \nabla\zeta\right)$, represents the vertical variability of geostrophic absolute vorticity advection. $\overrightarrow{V_g}$ signals the geostrophic wind. The second term ② on the right side $\overrightarrow{V_g} \cdot \nabla\left(\frac{\partial \Phi}{\partial p}\right)$ is Laplace of geostrophic temperature advection, representing the temperature advection caused by the geostrophic wind. $\Phi = gZ$ is geopotential height. Within the quasi-geostrophic framework, these two forcing terms act independently and often offset each other. This mutual cancellation limits the effectiveness of the traditional ω equation in diagnosing vertical motion forcing in small-scale systems over complex terrain. Hoskins et al. (1978) proposes reformulation of the traditional ω equation. This approach combines the terms on the right side of Equation 3 into the divergence of the Q-vector, and defines the quasi-geostrophic Q-vector.

$$\vec{Q} = (Q_x, Q_y) = -\frac{R}{p}\left(\frac{\partial \overrightarrow{V_g}}{\partial x} \cdot \nabla T, \frac{\partial \overrightarrow{V_g}}{\partial y} \cdot \nabla T\right) \quad (4)$$

R is the gas constant for dry air is approximately 287 J kg^{-1} K^{-1}. Based on the static equilibrium equation, the state equation, the geostrophic wind relationship, and the thermal wind relationship in the p-coordinate, it can be proved:

$$\left(\sigma\nabla^2 + f^2\frac{\partial^2}{\partial p^2}\right)\omega = -2\nabla \cdot \vec{Q} \quad (5)$$

The detailed derivation process can be found in Yao et al. (2012). To account for the non-geostrophic effect, this study replaces the geostrophic wind $\overrightarrow{V_g}$ with the actual wind $\vec{V}$, obtaining the non-geostrophic Q-vector and its expanded component form.

$$\vec{Q} = (Q_x, Q_y) = -\frac{R}{p}\left(\frac{\partial \vec{V}}{\partial x} \cdot \nabla T, \frac{\partial \vec{V}}{\partial y} \cdot \nabla T\right) \quad (6)$$

$$Q_x = -\frac{R}{p}\left(\frac{\partial u}{\partial x}\frac{\partial T}{\partial x} + \frac{\partial v}{\partial x}\frac{\partial T}{\partial y}\right) \quad (7)$$

21698996, 2026, 21, Downloaded from https://agupubs.onlinelibrary.wiley.com/doi/10.1029/2026JD047900 by Aiming Huang - Nanjing University , Wiley Online Library on [29/10/2026]. See the Terms and Conditions (https://onlinelibrary.wiley.com/terms-and-conditions) on Wiley Online Library for rules of use; OA articles are governed by the applicable Creative Commons License

$$Q_y = -\frac{R}{p}\left(\frac{\partial u}{\partial y}\frac{\partial T}{\partial x} + \frac{\partial v}{\partial y}\frac{\partial T}{\partial y}\right) \tag{8}$$

Equation 6 indicates that the magnitude of the Q-vector measures the intensity of the interaction between the deformation of the horizontal wind field and the temperature gradient. A larger magnitude represents stronger nonlinear coupling between the wind field and the thermal field, as well as stronger vertical motion forcing. The Q-vector direction points toward regions of ascending motion, where precipitation is most likely to occur.

Equations 7 and 8 define the Q-vector components in the x and y-direction, with the unit of $m^2\ kg^{-1}\ s^{-1}$. This study further calculates the Q-vector divergence $\nabla \cdot \vec{Q}$ of Equation 5, to diagnose low-level dynamical lifting induced by terrain relief. The unit of the Q-vector divergence is $s^{-3}\ Pa^{-1}$. When $\nabla \cdot \vec{Q} > 0$, it indicates local air divergence and suppresses convective development. When $\nabla \cdot \vec{Q} < 0$, it indicates local air convergence, which favors upward motion and convective initiation. Compared with the compensating forcing terms in the traditional ω equation, Q-vector divergence provides a clear forcing signal. This property facilitates the identification of the core region of vertical motion (Cao & Gao, 2007).

2.4.3. Baroclinic Vector

The baroclinic vector is used to describe the spatial non-uniformity of atmospheric baroclinicity, which can clearly reveal the influence of terrain-induced thermodynamic gradients on baroclinic instability (Q. Xu, 1992). The baroclinic vector B arises from the nonparallel alignment between isothermal surfaces and isobaric surfaces. It can be defined as:

$$B = \nabla\alpha \times \nabla p \tag{9}$$

Among them, $\alpha = \frac{1}{\rho}$ is the specific volume, ρ denotes density. Using the ideal gas Equation $p = \rho RT$, the specific volume is expressed as $\alpha = \frac{RT}{p}$. Substitute this into Equation 9:

$$\nabla\alpha \times \nabla p = \nabla\left(\frac{RT}{p}\right) \times \nabla p = R\left(\frac{1}{p}\nabla T - \frac{T}{p^2}\nabla p\right) \times \nabla p = \frac{R}{p}\nabla T \times \nabla p - \frac{RT}{p^2}(\nabla p \times \nabla p) \tag{10}$$

Because $\nabla p \times \nabla p = 0$, the baroclinic vector simplifies to the form:

$$\nabla\alpha \times \nabla p = \frac{R}{p}\nabla T \times \nabla p \tag{11}$$

This study focuses on the contribution of the horizontal temperature gradient to the atmospheric baroclinicity. Following Martin (2006, 2014), pressure gradient variations are filtered out. The vertical unit vector is cross-multiplied to retain only the direction information of the pressure gradient.

$$B = \frac{R}{p}\nabla T \times \kappa \tag{12}$$

$$B_x = \frac{R}{p}\frac{\partial T}{\partial x} \tag{13}$$

$$B_y = \frac{R}{p}\frac{\partial T}{\partial y} \tag{14}$$

∇T is a horizontal temperature gradient, and κ denotes the vertical unit vector. Equations 13 and 14 define the x and y-components of the baroclinic vector, with the unit of $m^2\ kg^{-1}$. Therefore, the baroclinic vector B is used to quantify the intensity and direction of atmospheric baroclinicity.

21698996, 2026, 21, Downloaded from https://agupubs.onlinelibrary.wiley.com/doi/10.1029/2026JD047900 by Anning Huang - Nanjing University , Wiley Online Library on [29/10/2026]. See the Terms and Conditions (https://onlinelibrary.wiley.com/terms-and-conditions) on Wiley Online Library for rules of use; OA articles are governed by the applicable Creative Commons License

21698996, 2026, 21, Downloaded from https://agupubs.onlinelibrary.wiley.com/doi/10.1029/2026JD047900 by Anming Huang - Nanjing University , Wiley Online Library on [29/10/2026]. See the Terms and Conditions (https://onlinelibrary.wiley.com/terms-and-conditions) on Wiley Online Library for rules of use; OA articles are governed by the applicable Creative Commons License

2.4.4. Temperature Advection

Although temperature gradients affect the atmospheric baroclinicity, the atmospheric thermal state is not static. The wind field continuously transports heat. Temperature advection describes the transport of local temperature caused by the horizontal wind within a given area.

$$\text{Temperature Advection} = -\overrightarrow{V} \cdot \nabla T \tag{15}$$

In Equation 15, when the wind blows from a cold region toward a warm region, the temperature advection $-\overrightarrow{V} \cdot \nabla T < 0$ is negative, indicating cold advection. Conversely, wind blows from a warm region toward a cold region, the temperature advection $-\overrightarrow{V} \cdot \nabla T > 0$ becomes positive, indicating warm advection. The unit of temperature advection is 10^{-5} K s^{-1}.

3. Results

3.1. Model Evaluation

This study first evaluates the simulation performance of the atmospheric circulation configuration and composite mean precipitation associated with RHEP. Under P1, the South Asia High at 200 hPa in the CTL experiment has a slightly larger spatial extent than the observations. However, both the location and intensity of the South Asia High are reasonably reproduced. The CTL experiment reasonably simulates the westerly trough with the location of the western SCB at 500 hPa and the southwest vortex located in the western SCB at 700 hPa under P1. Southerly winds transport the water vapor toward the western SCB in the CTL experiment, matching observations. Consequently, the CTL experiment reproduces the spatial distribution of the composite mean precipitation under P1 with a spatial correlation coefficient of 0.56 between the observations and simulation, which is significant at the 0.05 level (Figures 3a and 3c).

Under P2, the CTL experiment replicates the South Asia High at 200 hPa, with the core covering the southern TP, consistent with the observations. While the westerly trough at 500 hPa and the southwest vortex at 700 hPa over the central-eastern SCB produced by the CTL experiment are relatively weaker than the observations, the locations of both systems are captured reasonably well. The observations show southwesterly winds transporting water vapor from the Bay of Bengal toward the central-eastern SCB under P2; this feature is also well simulated by the CTL experiment. Although the CTL experiment underestimates the magnitude of the GPM-derived composite mean precipitation under P2, it reasonably captures the spatial pattern, with a spatial correlation coefficient of 0.41 between CTL and GPM, significant at the 0.05 level (Figures 3b and 3d). Overall, the CTL experiment can accurately reproduce both the atmospheric circulation configuration and the spatial distribution of composite mean precipitation under both P1 and P2.

3.2. The Influence of Terrain Relief on RHEP Over the SCB

Under P1, the CTL experiment exhibits two primary precipitation centers over the southwestern and northwestern SCB, with composite mean precipitation exceeding 80 mm (Figure 4a). Compared with the CTL experiment, the TP_NM experiment without the terrain relief over the TP displays a marked reduction in composite mean precipitation, primarily confined to the southwestern SCB (Figure 4b). These results indicate that terrain relief over the TP increases composite mean precipitation over the western SCB. The regional mean precipitation (102°E–106°E, 29°N–33°N) in the CTL experiment increases by 20.3% relative to the TP_NM experiment, with positive anomalies exceeding 30 mm concentrated in the western SCB under statistically significant at the 95% confidence level (Figure 4d). Furthermore, the mean duration of RHEP is prolonged by 3.4 hr, and the mean intensity is increased by 0.38 mm hr^{-1} due to the terrain relief over the TP (Figure 4f).

Under P1, the YG_NM experiment without the terrain relief over the Yunnan–Guizhou Plateau shows a reduced extent of the composite mean precipitation center in the southwestern and northwestern SCB compared with the CTL experiment (Figures 4a and 4c), indicating that the terrain relief over the Yunnan–Guizhou Plateau increases composite mean precipitation over the western SCB. The regional mean precipitation (102°E–106°E, 29°N–33°N) in the CTL experiment increases by 10.9% relative to the YG_NM experiment, with positive anomaly centers exceeding 30 mm in the western SCB (Figure 4e). The significant anomalies are mainly

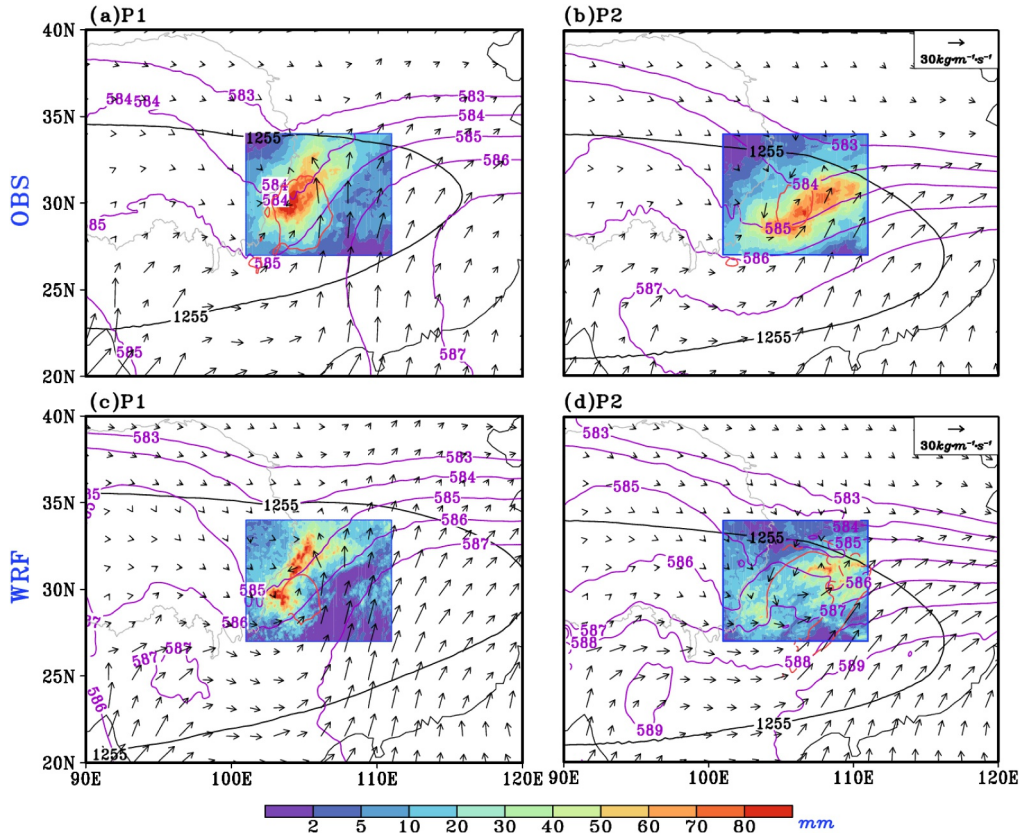


Figure 3. Comparison of the CTL simulation with GPM precipitation data and ERA5 atmospheric reanalysis in terms of mean precipitation and atmospheric circulation during the selected regional hourly extreme precipitation events over the Sichuan Basin under each dominant synoptic pattern. The shading represents the mean precipitation (shading, unit: mm) from the CTL experiment and GPM IMERGE. The black line symbolizes the South Asia high at 200 hPa, and the purple contour depicts the geopotential height (unit: degpm) at 500 hPa. The red contour represents the southwest vortex at 700 hPa. The vector displays the vertically integrated (surface-300 hPa) water vapor flux (unit: kg m^{-1} s^{-1}). The atmospheric circulation data are derived from ERA5.

distributed over the western SCB, indicating an enhancement of precipitation associated with the terrain relief over the Yunnan–Guizhou Plateau under P1. The terrain relief over the Yunnan–Guizhou Plateau prolongs the mean duration by 0.6 hr and increases the mean intensity by 0.24 mm hr^{-1} under P1 (Figure 4f).

Under P2, the composite mean precipitation in the CTL experiment is primarily concentrated over the eastern SCB, with a core precipitation amount exceeding 50 mm (Figure 4g). Compared with the CTL experiment, the TP_NM experiment without terrain relief over the TP shows a limited decrease in composite mean precipitation over the eastern SCB (Figure 4h). The regional mean precipitation (106°E–110°E, 29°N–32.5°N) in the CTL experiment increases by only 2.5% relative to the TP_NM experiment, with the precipitation difference showing alternating positive and negative patterns. The positive anomaly centers primarily occur around 107.5°E and 31°N, with central differences exceeding 30 mm (Figure 4j). However, the statistically significant areas are relatively limited, suggesting that the precipitation response to the terrain relief over the TP under P2 is weaker than that under P1. The increase in the composite mean precipitation is attributed to the prolonged duration of RHEP by 1.3 hr and increased intensity by 0.07 mm hr^{-1} due to the terrain relief over the TP under P2 (Figure 4l).

Under P2, the YG_NM experiment without terrain relief over the Yunnan–Guizhou Plateau exhibits a marked increase in composite mean precipitation over the eastern SCB compared to the CTL experiment (Figures 4g and 4i). The result indicates that the terrain relief over the Yunnan–Guizhou Plateau slightly decreases the composite mean precipitation in the CTL experiment. In particular, the regional mean precipitation over the eastern SCB (106°E–110°E, 29°N–32.5°N) decreases by 3.3%, with a pronounced negative anomaly exceeding −20 mm centered in this region. This response is statistically significant at the 95% confidence level and is attributed to the

21698996, 2026, 21, Downloaded from https://agupubs.onlinelibrary.wiley.com/doi/10.1029/2026JD047900 by Anming Huang - Nanjing University , Wiley Online Library on [29/10/2026]. See the Terms and Conditions (https://onlinelibrary.wiley.com/terms-and-conditions) on Wiley Online Library for rules of use; OA articles are governed by the applicable Creative Commons License

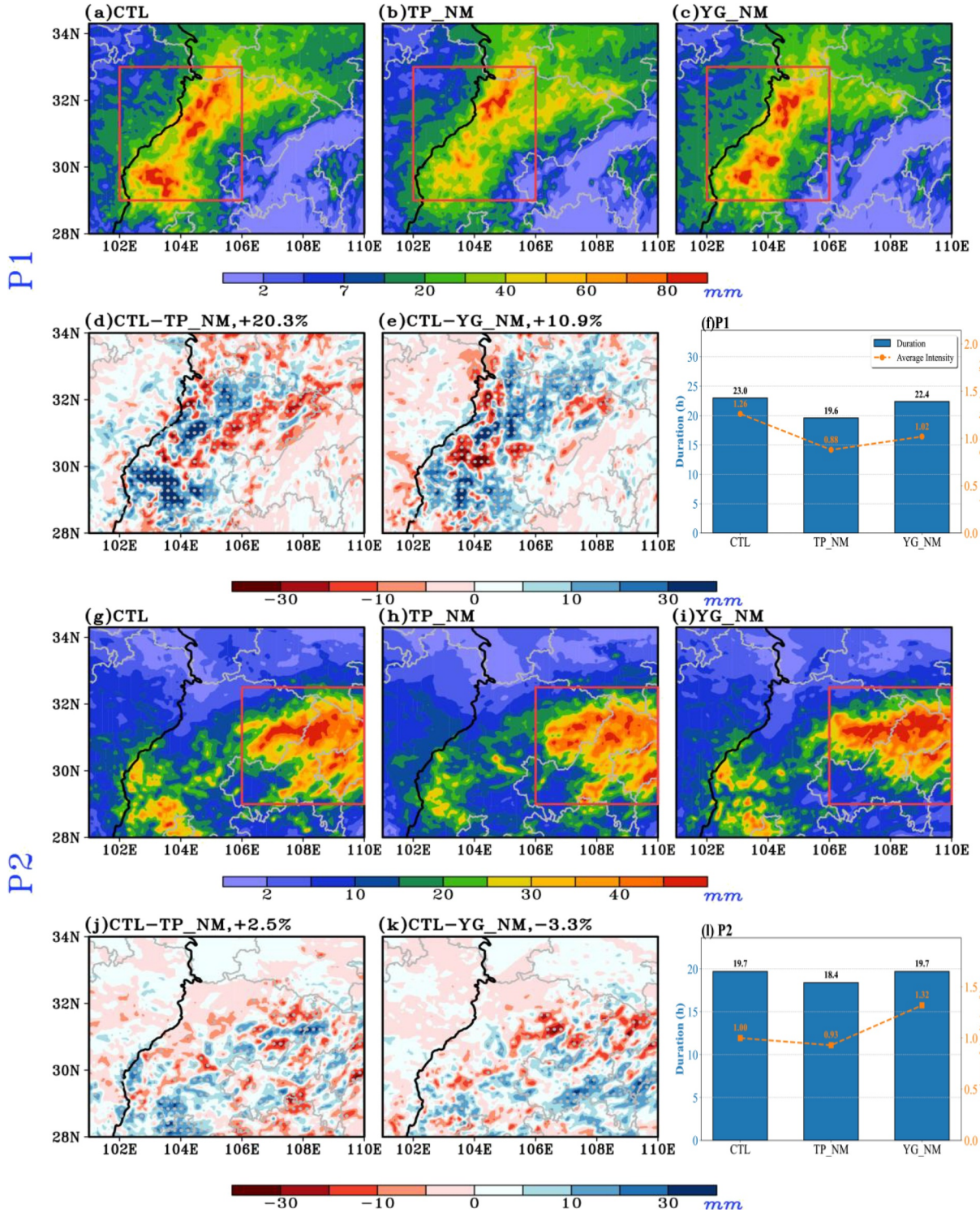


Figure 4. Comparison of precipitation among different experiments. Shading in panels (a–c, g–i) represents the composite mean precipitation amount (unit: mm) of regional hourly extreme precipitation (RHEP) over the Sichuan Basin from the CTL experiment and sensitivity experiments under the two dominant synoptic patterns. The red rectangle indicates the precipitation center focused on in this study. Shading in panels (d, e, j, k) represents the differences in composite mean precipitation between CTL and each sensitivity experiment. Gray dots in panels (d), (e), (j), and (k) mark grid points where the precipitation differences are significant at the 95% confidence level based on a Student's *t*-test. The numbers in the upper-left corner indicate the relative differences in regional mean precipitation between CTL and each sensitivity experiment. The regions bounded by 102°E–106°E, 29°N–33°N under P1 and 106°E–110°E, 29°N–32.5°N under P2 are used to calculate regional mean precipitation, consistent with the red rectangles. Panels (f) and (l) show the mean duration (bars, unit: hours) and mean intensity (lines, unit: mm hr^{-1}) of RHEP simulated by CTL and the sensitivity experiments under the two synoptic patterns.

21698996, 2026, 21, Downloaded from https://agupubs.onlinelibrary.wiley.com/doi/10.1029/2026JD047900 by Anning Huang - Nanjing University , Wiley Online Library on [29/10/2026]. See the Terms and Conditions (https://onlinelibrary.wiley.com/terms-and-conditions) on Wiley Online Library for rules of use; OA articles are governed by the applicable Creative Commons License

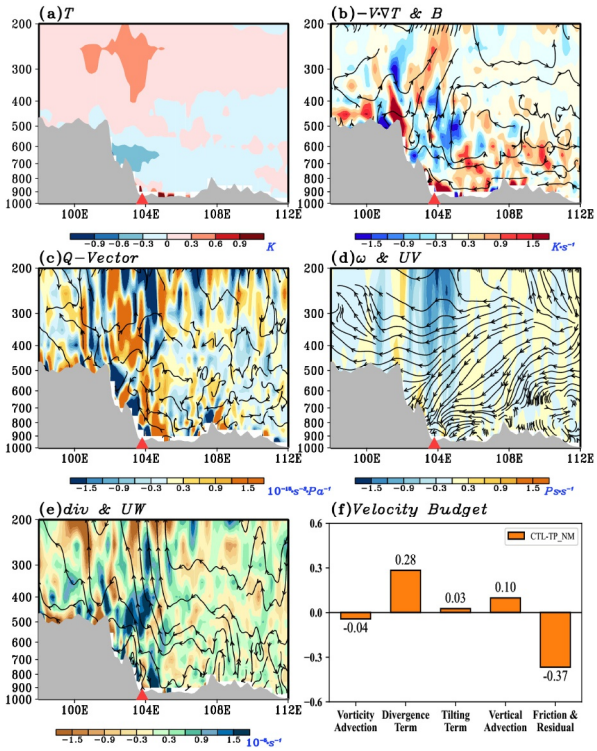


Figure 5. The pressure-longitude cross sections the 29.5°N of the differences between the CTL and TP_NM experiments for the air temperature (shading, unit: K) (a); the temperature advection (shading, unit: 10^{-5} K s^{-1}) and baroclinic vector (stream, unit: m^2 kg^{-1}) (b); the *Q*-vector (stream, unit: m^2 kg^{-3} s^{-1}) and *Q*-vector divergence (shading, unit: s^{-3} Pa^{-1}) (c); the vertical velocity (shading, unit: Pa s^{-1}) and wind vector with *x* and *y* component (vector, unit: m s^{-1}) (d); the divergence (shading, unit: 10^{-5} s^{-1}) and wind vector with *x* and *z* component (vector, unit: m s^{-1}); each term of vorticity budget equation (bar, unit: s^{-2}) at 700 hPa under P1. The red triangle indicates the area with abnormal precipitation. The gray shading indicates the terrain.

terrain relief of the Yunnan–Guizhou Plateau (Figure 4k). This decreased composite mean precipitation is attributed to the decrease in the mean intensity of RHEP by 0.32 mm hr^{-1} induced by the terrain relief over the Yunnan–Guizhou Plateau under P2 (Figure 4l).

3.3. The Mechanism of the Dynamic and Thermal Influence of Terrain Relief on RHEP Over SCB Under P1

The analysis of the influencing mechanisms employed the results from the CTL experiment minus those from each sensitivity experiment, demonstrating the effects of terrain relief on the TP and the Yunnan–Guizhou Plateau. Under P1, the westerly trough at 500 hPa and the southwest vortex at 700 hPa are located in the western SCB, with southerly winds transporting moisture into the region. The southeasterly winds prevail along the windward slope of the western SCB.

Compared with the TP_NM experiment under P1, the retained terrain relief over the TP first induces low-level southeasterly wind anomalies over the western SCB and adjacent windward slope, accompanied by warm temperature-advection anomalies in this region (Figure S3a in Supporting Information S1). This flow adjustment further enhances anomalous moisture transport toward the western SCB and strengthens moisture convergence there (Figure S4a in Supporting Information S1). These terrain-induced low-level flow, thermal-advection, and moisture-convergence anomalies promote the following local thermodynamic and dynamic responses associated with RHEP.

From a thermal perspective, the terrain relief over the TP traps warm and humid moisture at 950 hPa in SCB, and cools the air at 600 hPa over the eastern edge of the TP in the CTL experiment (Figure 5a). These lead to an abnormal cold advection of -0.9×10^{-5} K s^{-1} near 600 hPa, and an abnormal warm advection of 1.5×10^{-5} K s^{-1} near 950 hPa over the western SCB under P1 (Figure 5b). Under the impact of the terrain relief of the TP, the intensified vertical temperature gradient and enhanced atmospheric baroclinity deepen the westerly trough at 500 hPa over the western SCB, which promotes ascending motion with convergence in the middle and lower troposphere there under P1 (Figures 5a and 5b).

From the dynamic perspective, the terrain relief over the TP induces low-level air convergence and vertical-motion forcing, corresponding with the large Q-vector divergence abnormality values of -1.5×10^{-15} s^{-3} Pa^{-1} near 950 hPa and $1.5 \times 10^{-15} s^{-3}$ Pa^{-1} above 700 hPa (Figure 5c). The terrain relief induces an anomalous easterly wind component (the prevailing wind on the windward slope) and a large vertical velocity negative abnormality of -1.5×10^{-15} Pa s^{-1} over the western SCB under P1 (Figure 5d). Meanwhile, the anomalous convergence of div at low levels and anomalous divergence of div at high levels, corresponding to the vertical ascending air current due to the terrain relief over the TP under P1 (Figure 5e). The enhanced easterly wind component, moisture convergence, and ascending air over western SCB augment the divergence term in the vorticity budget equation, ultimately strengthening the southwest vortex (Figure 5f). The deepened westerly trough and strengthened southwest vortex prolong the average duration and increase the average intensity of RHEP in the western SCB due to the terrain relief over the TP under P1 (Figures 3c and 4f).

The mechanism by which the terrain relief of the Yunnan–Guizhou Plateau influences the RHEP over SCB is similar to that of the TP. The terrain relief over the Yunnan–Guizhou Plateau modifies the low-level inflow along the southern SCB and produces the warm temperature-advection anomalies near the western SCB (Figure S3b in Supporting Information S1). The corresponding moisture response is spatially mixed, with both moisture convergence and divergence anomalies around the western SCB (Figure S4b in Supporting Information S1). The Yunnan–Guizhou Plateau terrain relief affects low-level wind and moisture variation and subsequent thermodynamic and dynamic responses.

21698996, 2026, 21, Downloaded from https://agupubs.onlinelibrary.wiley.com/doi/10.1029/2026JD047900 by Anning Huang - Nanjing University , Wiley Online Library on [29/10/2026]. See the Terms and Conditions (https://onlinelibrary.wiley.com/terms-and-conditions) on Wiley Online Library for rules of use; OA articles are governed by the applicable Creative Commons License

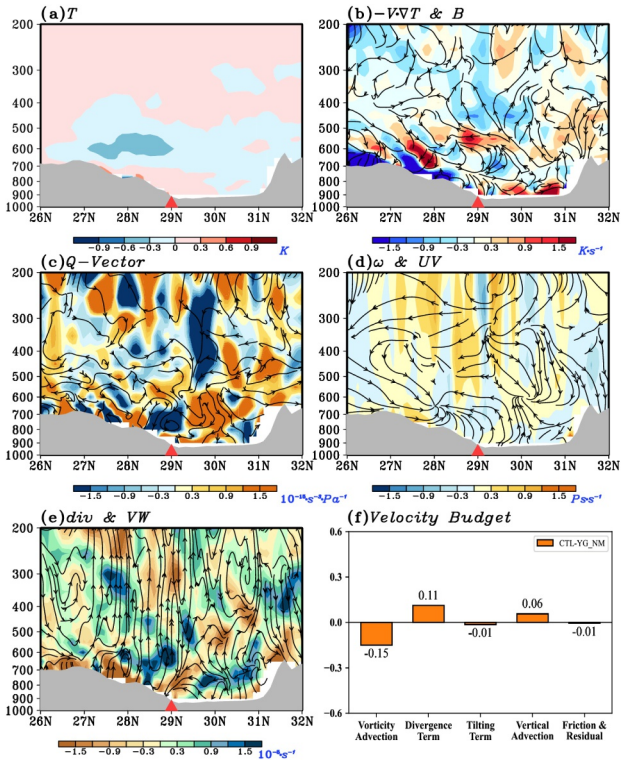


Figure 6. The pressure-latitude cross sections along 104°E of the differences between the CTL and YG_NM experiments for variables the same as Figure 5 under P1.

From a thermal perspective, the terrain relief over the Yunnan–Guizhou Plateau warms the air by 0.3 K near 950 hPa and cools the air by 0.5 K near 600 hPa over western SCB (Figure 6a). The anomalous temperature advection induced by the terrain relief over the Yunnan–Guizhou Plateau shows a warm anomaly exceeding 0.9×10^{-5} K s^{-1} near 950 hPa and a cold anomaly exceeding -0.6×10^{-5} K s^{-1} near 600 hPa, leading to a large vertical temperature gradient (Figure 6b). The enhanced atmospheric baroclinity near 104°E, 29°N due to this vertical temperature gradient deepens the westerly trough at 500 hPa, promoting air convergence in the middle and lower troposphere over the western SCB under P1 (Figure 6b).

From the dynamic perspective, the terrain relief over the Yunnan–Guizhou Plateau enhances low-level dynamical forcing over the western SCB under P1. At approximately 104°E and 29°N, the terrain-induced dynamic forcing produces negative Q-vector divergence abnormality values of -1.5×10^{-15} s^{-3} Pa^{-1} at lower levels, increasing the air convergence over the western SCB (Figure 6c). Additionally, the terrain relief of the Yunnan–Guizhou Plateau amplifies the southerly wind and induces the negative vertical velocity anomaly at low level under P1 (Figure 6d). The enhancement in the prevailing easterly wind component on the windward slope, combined with the low-level convergence and high-level divergence in div distribution, results in an abnormal upward airflow over western SCB due to the terrain relief over the Yunnan–Guizhou Plateau (Figure 6e), leading to a positive anomaly of the divergence term in the vorticity budget equation and a strengthened southwest vortex over western SCB (Figure 6g). The terrain relief of the Yunnan–Guizhou Plateau deepens the westerly trough and enhances the southwest vortex, ultimately prolonging the mean duration and increasing the mean intensity of RHEP over western SCB under P1 (Figures 3c and 4f). Furthermore, as the Yunnan–Guizhou Plateau lies to the southwest of the SCB, its terrain relief can block moisture transported by the southwest and southerly winds under P1, leading to a negative anomaly in the vorticity advection term between the CTL and YG_NM experiments (Figure 6f). This accounts for the limited influence on RHEP over western SCB under P1 due to the terrain relief over the Yunnan–Guizhou Plateau.

In summary, the terrain relief over the TP and Yunnan–Guizhou Plateau induces the low-level flow anomaly and enhances the atmospheric baroclinity, which further leads to the deepened westerly trough over the western SCB. Additionally, the terrain relief induces low-level convergence, vertical-motion forcing, and mechanical uplift, strengthening the divergence term in the vorticity budget equation and reinforcing the southwest vortex. The combination of these factors finally extends the duration and increases the intensity of RHEP in the western SCB under P1.

3.4. The Mechanism of the Dynamic and Thermal Influence of Terrain Relief on RHEP Over SCB Under P2

Under P2, the westerly trough at 500 hPa and the southwest vortex at 700 hPa situate the central-eastern SCB, and southwesterly winds transport moisture into this region. The windward slope of the eastern SCB experiences prevailing southwesterly winds.

Compared with the TP_NM experiment under P2, the terrain relief conducts low-level wind and temperature-advection anomalies over the eastern SCB that are weaker and localized than those under P1 (Figure S3c in Supporting Information S1). The moisture diagnosis also shows localized moisture-convergence anomalies over the eastern SCB (Figure S4c in Supporting Information S1). These weak flow, thermal-advection, and moisture-convergence responses are consistent with the limited enhancement of RHEP by TP terrain relief under P2.

From a thermal perspective, the terrain relief over the TP warms the near-surface air over the TP, producing a 0.9 K warm anomaly (Figure 7a). The abnormal warm air over the TP is advected eastward by the 500-hPa westerly flow, generating anomalous warm advection in the middle and upper troposphere over the eastern

21698996, 2026, 21, Downloaded from https://agupubs.onlinelibrary.wiley.com/doi/10.1029/2026JD047900 by Anning Huang - Nanjing University , Wiley Online Library on [29/10/2026]. See the Terms and Conditions (https://onlinelibrary.wiley.com/terms-and-conditions) on Wiley Online Library for rules of use; OA articles are governed by the applicable Creative Commons License

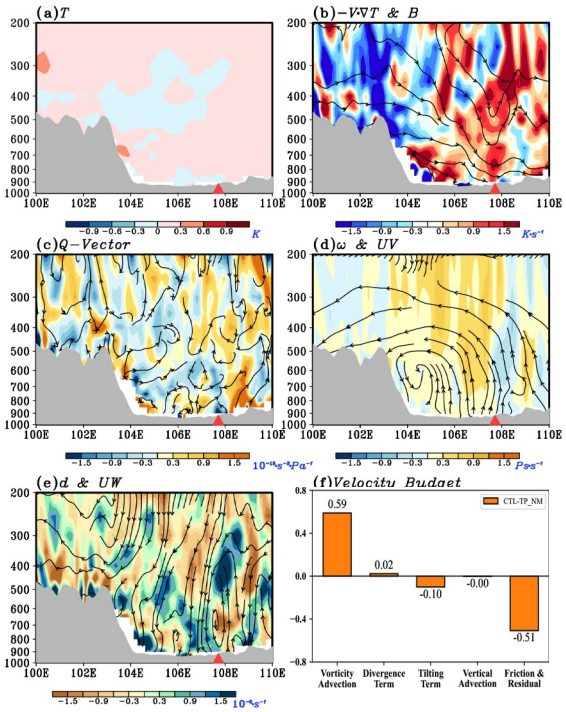


Figure 7. The pressure-longitude cross sections along 31°E of the differences between the CTL and TP_NM experiments for variables the same as Figure 5 under P2.

SCB due to the terrain relief over the TP under P2 (Figure 7b). The enhanced warm advection intensifies the vertical temperature gradient over the eastern SCB, strengthens the atmospheric baroclinity, and thereby enhances the westerly trough under P2 due to the terrain relief over the TP (Figures 3d and 7b).

From a dynamic perspective, low-level air disturbances generate a negative Q-vector divergence anomaly at the lower levels, thereby promoting dynamic uplift of the air near 107.5°E, 31°N due to the terrain relief over the TP under P2 (Figure 7c). Meanwhile, these terrains generate an anomalous westerly wind component (the prevailing wind on the windward slope) at low levels and a negative vertical velocity anomaly near 107.5°E, 31°N (Figure 7d). The enhanced prevailing wind on the windward slope induces the anomalous vertical cyclone and the low-level convergence and high-level divergence in div distribution, which promotes the air ascent near 107.5°E 31°N due to the terrain relief over the TP under P2 (Figure 7e). As a result, positive anomalies in the vorticity advection term dominate the vorticity budget and strengthen the southwest vortex caused by the terrain relief over the TP under P2 (Figure 7g). The deepened westerly trough and strengthened southwest vortex prolong the mean duration and increase the mean intensity of RHEP over the eastern SCB due to the terrain relief over the TP under P2 (Figures 3d and 4l). However, the *Q*-vector divergence anomaly and vertical velocity anomaly under P2 are smaller than those under P1, which explains the limited influence of the terrain relief over the TP on RHEP under P2 (Figures 5c, 5d, 7c, and 7d).

The terrain relief over the Yunnan–Guizhou Plateau exerts an opposite influence on RHEP over the eastern SCB under P2 relative to P1. The Yunnan–Guizhou Plateau lies along the primary moisture transport pathway toward the SCB under P2.

Relative to the YG_NM experiment under P2, the retained terrain relief over the Yunnan–Guizhou Plateau clearly induces the low-level air anomalous northwest wind over the eastern SCB and produces cold temperature-advection anomalies over there (Figure S3d in Supporting Information S1). Meanwhile, positive moisture-flux divergence anomalies appear near the eastern SCB, indicating weakened moisture convergence and reduced moisture supply (Figure S4d in Supporting Information S1). These anomalies directly reflect in the subsequent thermodynamic and dynamic responses.

From a thermal perspective, the terrain relief warms the near-surface air while blocking the moisture transport into the SCB under P2 (Figure 8a). The terrain relief over the Yunnan–Guizhou Plateau induces a cold anomaly of 0.6 K over the SCB under P2 (Figure 8a). As a result, the terrain relief over the Yunnan–Guizhou Plateau produces anomalous cold advection of −1.5 K over the SCB, which reduces atmospheric baroclinicity and weakens the westerly trough under P2 (Figures 3d and 8b).

From a dynamic perspective, although the terrain relief on the Yunnan–Guizhou Plateau produces local near-surface flow perturbations, the weakened southerly wind leads to a positive *Q*-vector divergence anomaly of 1.5×10^{-15} s^{-3} Pa^{-1}, the negative vertical velocity anomaly of 0.9 Pa s^{-1} over the eastern SCB, indicating suppressed dynamic ascent (Figures 8c and 8d). The terrain relief on the Yunnan–Guizhou Plateau induces the anomalous northerly wind and inspires the vertical anticyclone near 107°N, 30°E–31°N, corresponding with the descending air over the eastern SCB (Figure 8e). The presence of terrain relief enhances the near-surface frictional dissipation and residual terms, leading to positive anomalies in this component (Figure 8g). In contrast, all remaining terms in the vorticity budget show negative anomalies due to blocked warm and humid inflow (Figure 8g). These negative anomalies indicate a weakened southwest vortex, reducing the mean intensity of RHEP and ultimately decreasing the precipitation over the eastern SCB (Figures 3d and 4l).

In general, the terrain relief over the TP has a limited impact on the mean duration and mean intensity of RHEP over eastern SCB under P2. The influence of terrain relief over the TP on the RHEP over eastern SCB is similar to that under P1, but weaker low-level convergence and vertical-motion forcing over the eastern SCB limit the

21698996, 2026, 21, Downloaded from https://agupubs.onlinelibrary.wiley.com/doi/10.1029/2026JD047900 by Anning Huang - Nanjing University , Wiley Online Library on [29/10/2026]. See the Terms and Conditions (https://onlinelibrary.wiley.com/terms-and-conditions) on Wiley Online Library for rules of use; OA articles are governed by the applicable Creative Commons License

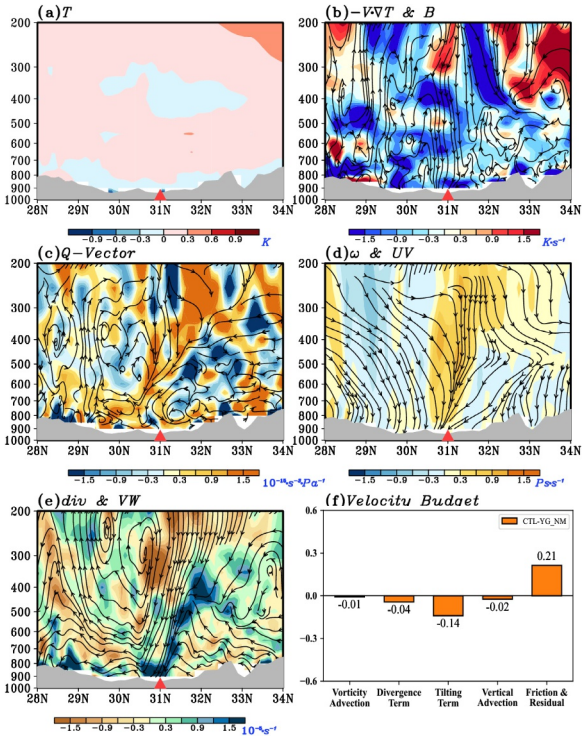


Figure 8. The pressure-latitude cross sections along 107°E of the differences between the CTL and YG_NM experiments for variables the same as Figure 5 under P2.

enhancement. In contrast, the terrain relief over the Yunnan–Guizhou Plateau blocks the moisture transport associated with the southwesterly wind and weakens the westerly trough under P2. The strengthened anomalous northerly winds over the eastern SCB suppress the southwest vortex. This suppression leads to a decrease in the mean intensity of RHEP under P2.

4. Results and Discussion

This study conducts sensitivity experiments using the WRF model to investigate the influence mechanism of terrain relief over the TP and Yunnan–Guizhou Plateau on the summer RHEP over the SCB under two dominant synoptic patterns. The main conclusions are as follows:

The terrain relief over the TP and Yunnan–Guizhou Plateau can affect the duration and intensity of RHEP over the SCB. Under P1, the terrain relief over the TP (Yunnan–Guizhou Plateau) can increase the RHEP amount in the western SCB by 20.3% (10.9%). Meanwhile, the mean duration of RHEP can be prolonged by 3.4 hr (0.6 hr), and the mean RHEP intensity can be enhanced by 0.38 mm hr^{-1} (0.24 mm hr^{-1}) over the western SCB due to the terrain relief over the TP (Yunnan–Guizhou Plateau). Mechanism analysis shows that the terrain relief directly affects the abnormal southeasterly wind in the low-level and the water vapor transport under P1 (Figure 9a). From a thermal perspective, the terrain relief over the TP (Yunnan–Guizhou Plateau) strengthens the westerly trough by increasing the vertical temperature gradient and atmospheric baroclinicity. From a dynamic perspective, the terrain relief over the TP (Yunnan–Guizhou Plateau) induces low-level convergence, vertical-motion forcing, anomalous easterly (southerly) winds, and further strengthens the southwest vortex (Figure 9b). The strengthened westerly trough and southwest vortex induced by the terrain

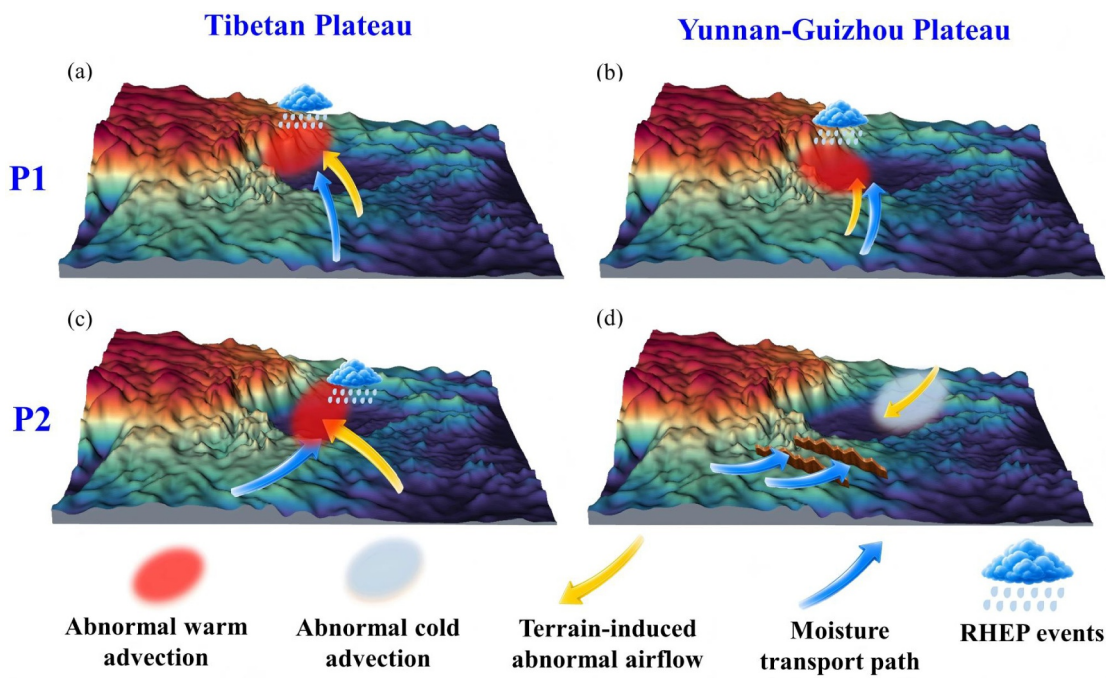


Figure 9. Illustrative diagram of terrain relief over the Tibetan Plateau and Yunnan–Guizhou Plateau differently modulates the regional hourly extreme precipitation events over the Sichuan Basin under the two dominant synoptic patterns.

21698996, 2026, 21, Downloaded from https://agupubs.onlinelibrary.wiley.com/doi/10.1029/2026JD047900 by Anning Huang - Nanjing University , Wiley Online Library on [29/10/2026]. See the Terms and Conditions (https://onlinelibrary.wiley.com/terms-and-conditions) on Wiley Online Library for rules of use; OA articles are governed by the applicable Creative Commons License

21698996, 2026, 21, Downloaded from https://agupubs.onlinelibrary.wiley.com/doi/10.1029/2026JD047900 by Anning Huang - Nanjing University , Wiley Online Library on [29/10/2026]. See the Terms and Conditions (https://onlinelibrary.wiley.com/terms-and-conditions) on Wiley Online Library for rules of use; OA articles are governed by the applicable Creative Commons License

relief over the TP (Yunnan–Guizhou Plateau) can prolong the duration and intensity of RHEP over the western SCB under P1. Since the Yunnan–Guizhou Plateau is located in the moisture path under P1, the terrain relief over the Yunnan–Guizhou Plateau weakly influences the RHEP over the western SCB compared to the TP.

Under P2, the terrain relief over the TP increases the mean precipitation of RHEP in the eastern SCB by 2.5%, which is attributed to the prolonged RHEP duration of 1.3 hr and a 0.07 mm hr^{-1} increase in RHEP intensity. Similar to the thermal influence mechanism under P1, the terrain relief of the TP intensifies the westerly trough in central-eastern SCB by the enhanced vertical temperature gradient and atmospheric baroclinity under P2. Additionally, the anomalous westerly winds at low level over the eastern SCB induced by the terrain relief over the TP strengthen the southwest vortex over central-eastern SCB. However, the terrain-induced low-level convergence and vertical-motion forcing by the terrain relief over the TP are relatively weaker under P2 than under P1. These account for the slightly increased mean precipitation over the eastern SCB under P2 (Figure 9c). In contrast, the terrain relief over the Yunnan–Guizhou Plateau can lead to a 3.3% reduction in the mean precipitation of RHEP over the eastern SCB, which is mainly attributed to a decrease in the RHEP intensity by 0.32 mm hr^{-1}. Further mechanism analysis indicates that the terrain relief over the Yunnan–Guizhou Plateau strengthens the anomalous northerly winds over eastern SCB, blocking the moisture brought by the southwesterly winds under P2. The reduced moisture weakens the atmospheric baroclinicity and, in turn, weakens the westerly trough over the central-eastern SCB. Meanwhile, the strengthened anomalous northerly winds and an anomalous vertical anticyclone cause the weakened southwest vortex and decreased RHEP intensity over the eastern SCB due to the terrain relief over the Yunnan–Guizhou Plateau under P2 (Figure 9d).

The findings of this study provide critical insights into the role of terrain relief in modulating the RHEP over SCB. These results hold significant implications for improving weather prediction models and can be applied to regional climate studies and risk assessments in similar mountainous regions. It should be noted that the model evaluation in this study is based on satellite-derived precipitation, which inevitably differs from in situ measurements. Future studies should therefore incorporate more station observations to further validate the simulated results. In addition, the study is limited by the scope of the model simulations, and further research is needed to explore the influence of additional terrain features and their interactions under different climate scenarios.

Conflict of Interest

The authors declare no conflicts of interest relevant to this study.

Availability Statement

The data set employed for this study is detailed below: (a) the GPM-IMERG precipitation data set, which has a spatial resolution of 0.1° (Hou et al., 2014). (b) The ERA5 reanalysis data set, characterized by a spatial resolution of 0.25°, is utilized in this study (Hersbach et al., 2020). (c) The data set from the National Centers for Environmental Prediction's final (FNL) global analysis, featuring a 1° horizontal resolution, is used in this research (National Centers for Environmental Prediction/National Weather Service/NOAA/U.S. Department of Commerce, 2000). (d) The numerical model (WRF) used in this study is version 4.2 (Skamarock et al., 2019).

Acknowledgments
This research is financially supported by the National Natural Science Foundation of China, with Grants 42505025 and U2342207, and the National Open Fund for Rainstorm Research (BYKJ2024Q02).

References

Ali, H., Fowler, H. J., Lenderink, G., Lewis, E., & Pritchard, D. (2021). Consistent large-scale response of hourly extreme precipitation to temperature variation over land. *Geophysical Research Letters*, *48*(4), e2020GL090317. https://doi.org/10.1029/2020GL090317

Bai, L., Liu, T., Sha, A., & Li, D. (2025). The spatiotemporal fluctuations of extreme rainfall and their potential influencing factors in Sichuan Province, China, from 1970 to 2022. *Remote Sensing*, *17*(5), 883. https://doi.org/10.3390/rs17050883

Barbero, R., Fowler, H. J., Blenkinsop, S., Westra, S., Moron, V., Lewis, E., et al. (2019). A synthesis of hourly and daily precipitation extremes in different climatic regions. *Weather and Climate Extremes*, *26*, 100219. https://doi.org/10.1016/j.wace.2019.100219

Cao, J., & Gao, S. (2007). Extended interpretations in Q vector analyses and applications in a torrential rain event. *Geophysical Research Letters*, *34*(15). https://doi.org/10.1029/2007GL030781

Chen, B., Huang, C., Gao, W., & Li, J. (2024). Analysis of the topographic influence on the flood-causing heavy rainfall process in western Sichuan Basin from August 14 to 18, 2020. *Plateau and Mountain Meteorology Research*, *44*(4), 41–53. https://doi.org/10.3969/j.issn.1674-2184.2024.04.005

Chen, Z., Du, Y., Vincent, C., Short, E., & Yang, H. (2025). Influence of coastal topography on offshore diurnal rainfall propagation dynamics: A linear gravity wave model approach. *Journal of the Atmospheric Sciences*, *82*(9), 1911–1927. https://doi.org/10.1175/JAS-D-24-0214.1

Cheng, Q., Jin, H., & Ren, Y. (2023). Persistent and nonpersistent regional extreme total, daytime, and night-time precipitation events over southwest China (1961–2019). *International Journal of Climatology*, *43*(5), 2150–2174. https://doi.org/10.1002/joc.7968

Deng, M., Lu, R., & Li, C. (2022). Contrasts between the interannual variations of extreme rainfall over western and eastern Sichuan in mid-summer. *Advances in Atmospheric Sciences*, *39*(6), 999–1011. https://doi.org/10.1007/s00376-021-1219-3

Fang, J., Yang, W., Luan, Y., Du, J., Lin, A., & Zhao, L. (2019). Evaluation of the TRMM 3B42 and GPM IMERG products for extreme precipitation analysis over China. *Atmospheric Research*, *223*, 24–38. https://doi.org/10.1016/j.atmosres.2019.03.001

Gu, W., Zhu, X., Meng, X., & Qiu, X. (2021). Research on the influence of small-scale terrain on precipitation. *Water*, *13*(6), 805. https://doi.org/10.3390/w13060805

Hersbach, H., Bell, B., Berrisford, P., Hirahara, S., Horanyi, A., Munoz-Sabater, J., et al. (2020). The ERA5 global reanalysis [Dataset]. *Quarterly Journal of the Royal Meteorological Society*, *146*(730), 1999–2049. https://doi.org/10.1002/qj.3803

Holton, J. R., & Hakim, G. J. (2013). *An introduction to dynamic meteorology* (Vol. 88). Academic Press. Retrieved from https://www.sciencedirect.com/book/monograph/9780123848666/an-introduction-to-dynamic-meteorology

Hoskins, B. J., Draghici, I., & Davies, H. C. (1978). A new look at the ω-equation. *Quarterly Journal of the Royal Meteorological Society*, *104*(439), 31–38. https://doi.org/10.1002/qj.49710443903

Hou, A. Y., Kakar, R. K., Neeck, S., Azarbarzin, A. A., Kummerow, C. D., Kojima, M., et al. (2014). The global precipitation measurement mission [Dataset]. *Bulletin of the American Meteorological Society*, *95*(5), 701–722. https://doi.org/10.1175/bams-d-13-00164.1

Houze, R. A., Jr. (2012). Orographic effects on precipitating clouds. *Reviews of Geophysics*, *50*(1), RG1001. https://doi.org/10.1029/2011RG000365

Hu, Y., Zhai, P., Liu, L., Chen, Y., & Liu, Y. (2015). Dominant large-scale atmospheric circulation systems for the extreme precipitation over the western Sichuan Basin in summer 2013. *Advances in Meteorology*, *2015*(1), 690363. https://doi.org/10.1155/2015/690363

Huang, D., & Gao, S. (2018). Impact of different reanalysis data on WRF dynamical downscaling over China. *Atmospheric Research*, *200*, 25–35. https://doi.org/10.1016/j.atmosres.2017.09.017

Ji, Z., Zhang, M., Lin, Y., & Huang, Y. (2026). Impacts of small-scale terrain on the organization of an extreme-rainfall-producing MCS over the southeastern coast of China. *Journal of Geophysical Research: Atmospheres*, *131*(17), e2026JD046986. https://doi.org/10.1029/2026JD046986

Li, J., Chen, H., Jiang, X., & Li, P. (2024). Diurnal variations of summer rainfall response to large-scale circulations and low-level winds over the Sichuan Basin. *Climate Dynamics*, *62*(3), 2041–2056. https://doi.org/10.1007/s00382-023-07009-w

Li, J., Lu, C., Chen, J., Zhou, X., Yang, K., Xu, X., et al. (2025). The combined effects of convective entrainment and orographic drag on precipitation over the Tibetan Plateau. *Science China Earth Sciences*, *68*(8), 2615–2630. https://doi.org/10.1007/s11430-024-1619-5

Li, L., & Zhang, R. (2023). Evolution mechanisms, impacts, and variations of the vortices originated from the Tibetan Plateau. *Earth-Science Reviews*, *242*, 104463. https://doi.org/10.1016/j.earscirev.2023.104463

Li, Q., Zheng, Y., Zhou, G., Zhu, Y., Liu, C., & Liu, Y. (2022). Diurnal variations of rainfall affected by complex topography based on high-density observation in Chongqing over southwest China. *Theoretical and Applied Climatology*, *148*(3), 1373–1394. https://doi.org/10.1007/s00704-021-03918-0

Liao, R., Liu, G., & Liu, H. (2025). Characteristics and causes of July extreme rainfall events in the Sichuan-Chongqing-Shaanxi region, China. *Theoretical and Applied Climatology*, *156*(8), 440. https://doi.org/10.1007/s00704-025-05672-z

Liu, L., Ran, L., & Gao, S. (2018). Analysis of the characteristics of inertia-gravity waves during an orographic precipitation event. *Advances in Atmospheric Sciences*, *35*(5), 604–620. https://doi.org/10.1007/s00376-017-7159-2

Martin, J. E. (2006). The role of shearwise and transverse quasigeostrophic vertical motions in the midlatitude cyclone life cycle. *Monthly Weather Review*, *134*(4), 1174–1193. https://doi.org/10.1175/MWR3114.1

Martin, J. E. (2014). Quasi-geostrophic diagnosis of the influence of vorticity advection on the development of upper level jet-front systems. *Quarterly Journal of the Royal Meteorological Society*, *140*(685), 2658–2671. https://doi.org/10.1002/qj.2333

Mo, S., Zhao, P., Zhao, C., Xiao, H., Wang, Y., Zhang, P., et al. (2024). Climatic precipitation efficiency and its dependence on environmental factors over the Sichuan Basin and adjacent regions, Southwest China. *Theoretical and Applied Climatology*, *155*(5), 3613–3629. https://doi.org/10.1007/s00704-024-04835-8

National Centers for Environmental Prediction/National Weather Service/NOAA/U.S. Department of Commerce. (2000). NCEP FNL Operational Model Global Tropospheric Analyses, continuing from July 1999 (Updated daily) [Dataset]. *Research Data Archive at the National Center for Atmospheric Research, Computational and Information Systems Laboratory*. https://doi.org/10.5065/D6M043C6

Ng, C. P., Zhang, Q., & Li, W. (2021). Changes in hourly extreme precipitation over Eastern China from 1970 to 2019 dominated by synoptic-scale precipitation. *Geophysical Research Letters*, *48*(5), e2020GL090620. https://doi.org/10.1029/2020GL090620

Nie, Y., & Sun, J. (2021). Synoptic-Scale circulation precursors of extreme precipitation events over Southwest China during the rainy season. *Journal of Geophysical Research: Atmospheres*, *126*(13), e2021JD035134. https://doi.org/10.1029/2021JD035134

Orlanski, I., & Sheldon, J. P. (1995). Stages in the energetics of baroclinic systems. *Tellus A*, *47*(5), 605–628. https://doi.org/10.3402/tellusa.v47i5.11553

Pielke, R. A., Sr. (2013). *Mesoscale meteorological modeling* (3rd ed., Vol. 98). Academic Press. ISBN: 978-0-12-385237-3.

Qian, T., Zhao, P., Zhang, F., & Bao, X. (2015). Rainy-season precipitation over the Sichuan basin and adjacent regions in southwestern China. *Monthly Weather Review*, *143*(1), 383–394. https://doi.org/10.1175/MWR-D-13-00158.1

Roe, G. H. (2005). Orographic precipitation. *Annual Review of Earth and Planetary Sciences*, *33*(1), 645–671. https://doi.org/10.1146/annurev.earth.33.092203.122541

Sanders, F. (1986). Explosive cyclogenesis in the west-central North Atlantic Ocean, 1981–84. Part I: Composite structure and mean behavior. *Monthly Weather Review*, *114*(10), 1781–1794. https://doi.org/10.1175/1520-0493(1986)114<1781:ECITWC>2.0.CO;2

Schröer, K., & Kirchengast, G. (2018). Sensitivity of extreme precipitation to temperature: The variability of scaling factors from a regional to local perspective. *Climate Dynamics*, *50*(11), 3981–3994. https://doi.org/10.1007/s00382-017-3857-9

Shen, C., Li, G., & Dong, Y. (2022). Vertical structures associated with orographic precipitation during warm season in the Sichuan Basin and its surrounding areas at different altitudes from 8-year GPM DPR observations. *Remote Sensing*, *14*(17), 4222. https://doi.org/10.3390/rs14174222

Shen, J., Xue, H., Ge, F., & Zhang, J. (2025). Understanding heavy precipitation prediction bias in the Sichuan Basin based on the China Meteorological Administration operational mesoscale model. *Quarterly Journal of the Royal Meteorological Society*, *151*(770), e4966. https://doi.org/10.1002/qj.4966

Skamarock, W. C., Klemp, J. B., Dudhia, J., Gill, D. O., Liu, Z., Berner, J., et al. (2019). A description of the advanced research WRF model version 4. National Center for Atmospheric Research: Boulder, CO, USA [Software]. *Zenodo*, *145*(145), 550. https://doi.org/10.5281/zenodo.10098038

Vosper, S. B., Ross, A. N., Renfrew, I. A., Sheridan, P., Elvidge, A. D., & Grubišić, V. (2018). Current challenges in orographic flow dynamics: Turbulent exchange due to low-level gravity-wave processes. *Atmosphere*, *9*(9), 361. https://doi.org/10.3390/atmos9090361

21698996, 2026, 21, Downloaded from https://agupubs.onlinelibrary.wiley.com/doi/10.1029/2026JD047900 by Anning Huang - Nanjing University , Wiley Online Library on [29/10/2026]. See the Terms and Conditions (https://onlinelibrary.wiley.com/terms-and-conditions) on Wiley Online Library for rules of use; OA articles are governed by the applicable Creative Commons License

Wang, Y., Yang, K., Zhou, X., Chen, D., Lu, H., Ouyang, L., et al. (2020). Synergy of orographic drag parameterization and high resolution greatly reduces biases of WRF-simulated precipitation in central Himalaya. *Climate Dynamics*, *54*(3), 1729–1740. https://doi.org/10.1007/s00382-019-05080-w

Wang, Y. J., Wu, J. P., Yin, F. K., Xu, X., Chen, T., Yang, X. R., et al. (2025). The impact of moist orographic gravity wave drag parameterization on summer circulation and heavy rainfall. *Journal of Geophysical Research: Atmospheres*, *130*(12), e2025JD043666. https://doi.org/10.1029/2025JD043666

Wu, A., & Li, G. (2022). Roles of the topographically-affected boundary layer low-level jet in the moisture transport process of nocturnal rainstorms in mountainous areas around the western Sichuan basin. *Atmosphere*, *14*(1), 84. https://doi.org/10.3390/atmos14010084

Wu, Y., Huang, A., Huang, D., Chen, F., Yang, B., Zhou, Y., et al. (2018). Diurnal variations of summer precipitation over the regions east to Tibetan Plateau. *Climate Dynamics*, *51*(11), 4287–4307. https://doi.org/10.1007/s00382-017-4042-x

Wu, Z., Liu, H., Chan, K. T., Wu, K., Zhang, W., & Wang, D. (2022). Effects of topography and latent heat on the evolution of a mesoscale dual-core southwest vortex over Sichuan Basin, China. *Frontiers in Earth Science*, *10*, 827601. https://doi.org/10.3389/feart.2022.827601

Xia, F., Huang, X., Fei, J., Wang, J., Cheng, X., & Zhang, C. (2025). Influence of synoptic pattern on the spatiotemporal features and diurnal variation of extremely persistent heavy rainfall over the Sichuan Basin, China. *Advances in Atmospheric Sciences*, *42*(3), 527–550. https://doi.org/10.1007/s00376-024-3358-9

Xia, R., Luo, Y., Zhang, D. L., Li, M., Bao, X., & Sun, J. (2021). On the diurnal cycle of heavy rainfall over the Sichuan Basin during 10–18 August 2020. *Advances in Atmospheric Sciences*, *38*(12), 2183–2200. https://doi.org/10.1007/s00376-021-1118-7

Xu, Q. (1992). Ageostrophic pseudovorticity and geostrophic C-Vector Forcing—A new look at the Q vector in three dimensions. *Journal of the Atmospheric Sciences*, *49*(12), 981–990. https://doi.org/10.1175/1520-0469(1992)049<0981:APAGCV>2.0.CO;2

Xu, X., Huang, A., Huang, D., Zhang, Y., Gu, C., Cai, S., et al. (2023). What are the dominant synoptic patterns leading to the summer regional hourly extreme precipitation events over central-eastern Tibetan Plateau and Sichuan Basin? *Geophysical Research Letters*, *50*(5), e2022GL102342. https://doi.org/10.1029/2022gl102342

Xu, X., Huang, A., Zhang, Y., Yang, X., & Zhao, W. (2025). Impact of large-scale topography surrounding the Sichuan Basin on its regional hourly extreme precipitation in summer under specific weather patterns: Multi-case study. *Journal of Geophysical Research: Atmospheres*, *130*(9), e2024JD042239. https://doi.org/10.1029/2024JD042239

Xu, X., Huang, A., Zhao, W., Yang, B., Xue, D., & Zhang, Y. (2024). Roles of the Tibetan Plateau and Yunnan-Guizhou Plateau in the regional extreme precipitation over Sichuan Basin in summer: A case study. *Journal of Geophysical Research: Atmospheres*, *129*(3), e2023JD039776. https://doi.org/10.1029/2023JD039776

Xu, Y., Li, G., Zhang, X., Xie, X., & Dong, Y. (2025). Relationship between a heavy rainfall and gravity wave in Sichuan Basin. *J Appl Meteor Sci*, *36*(1), 65–76. https://doi.org/10.11898/1001-7313.20250107

Yan, X., Chen, Q., Li, Y., & Liao, Y. (2025). Comparative analysis of summer deep convection systems over the Tibetan Plateau and Sichuan Basin. *Atmosphere*, *16*(10), 1134. https://doi.org/10.3390/atmos16101134

Yang, K. Q., Xiao, D. X., Jiang, X. W., Li, Z. R., & Fu, S. M. (2023). Mechanisms governing the formation and long-term sustainment of a northeastward moving southwest vortex. *Sustainability*, *15*(12), 9255. https://doi.org/10.3390/su15129255

Yang, M., Liu, G., Chen, T., Chen, Y., & Xia, C. (2020). Evaluation of GPM IMERG precipitation products with the point rain gauge records over Sichuan, China. *Atmospheric Research*, *246*, 105101. https://doi.org/10.1016/j.atmosres.2020.105101

Yao, Y., Yue, C., & Shou, S. (2012). *Q Vector principle and its application in the weather analysis and forecast*. China Meteorological Press.

Yepes, J., Mejía, J. F., Mapes, B., & Poveda, G. (2020). Gravity waves and other mechanisms modulating the diurnal precipitation over one of the rainiest spots on Earth: Observations and simulations in 2016. *Monthly Weather Review*, *148*(9), 3933–3950. https://doi.org/10.1175/MWR-D-19-0405.1

Yu, L., Fu, Y., Yang, Y., Pan, X., & Tan, R. (2020). Trumpet-shaped topography modulation of the frequency, vertical structures, and water path of cloud systems in the summertime over the southeastern Tibetan Plateau: A perspective of daytime–nighttime differences. *Journal of Geophysical Research: Atmospheres*, *125*(3), e2019JD031803. https://doi.org/10.1029/2019JD031803

Yuan, Y., Zhai, P., Chen, Y., & Li, J. (2021). Hourly extreme precipitation changes under the influences of regional and urbanization effects in Beijing. *International Journal of Climatology*, *41*(2), 1179–1189. https://doi.org/10.1002/joc.6784

Zhang, S., Liu, B., Ren, G., Zhou, T., Jiang, C., Li, S., & Su, B. (2021). Moisture sources and paths associated with warm-season precipitation over the Sichuan Basin in southwestern China: Climatology and interannual variability. *Journal of Hydrology*, *603*, 127019. https://doi.org/10.1016/j.jhydrol.2021.127019

Zhang, Y., Sun, J., Zhu, L., Tang, H., Jin, S., & Liu, X. (2021). Comparison of two types of persistent heavy rainfall events during sixteen warm seasons in the Sichuan Basin. *Atmospheric and Oceanic Science Letters*, *14*(6), 100094. https://doi.org/10.1016/j.aosl.2021.100094

Zhao, Y. (2015). A study on the heavy-rain-producing mesoscale convective system associated with diurnal variation of radiation and topography in the eastern slope of the western Sichuan plateau. *Meteorology and Atmospheric Physics*, *127*(2), 123–146. https://doi.org/10.1007/s00703-014-0356-y

Zhou, X. Y., & Lei, W. J. (2018). Complex patterns of precipitation and extreme events during 1951-2011 in Sichuan Basin, Southwestern China. *Journal of Mountain Science*, *15*(2), 340–356. https://doi.org/10.1007/s11629-016-4186-x

Zhou, Y., & Li, G. (2024). Evolution and roles of mesoscale convective system during the Nocturnal Rainfall in Sichuan Basin and its surrounding mountainous areas. *Dynamics of Atmospheres and Oceans*, *106*, 101445. https://doi.org/10.1016/j.dynatmoce.2024.101445

21698996, 2026, 21, Downloaded from https://agupubs.onlinelibrary.wiley.com/doi/10.1029/2026JD047900 by Anming Huang - Nanjing University , Wiley Online Library on [29/10/2026]. See the Terms and Conditions (https://onlinelibrary.wiley.com/terms-and-conditions) on Wiley Online Library for rules of use; OA articles are governed by the applicable Creative Commons License